

Microwave transitions in atomic sodium: Radiometry and polarimetry using the sodium layer

Mariusz Pawlak,^{1,*} Eve L. Schoen,^{2,3} Justin E. Albert,⁴ and H. R. Sadeghpour⁵

¹*Faculty of Chemistry, Nicolaus Copernicus University in Toruń, Gagarina 7, 87-100 Toruń, Poland*

²*Department of Physics, University of California,
366 Physics North MC 7300, Berkeley, California 94720, USA*

³*MIT Kavli Institute for Astrophysics and Space Research, Massachusetts Institute of Technology,
77 Massachusetts Ave, Cambridge, Massachusetts 02139, USA*

⁴*Department of Physics and Astronomy, University of Victoria, Victoria, British Columbia V8P 5C2, Canada*

⁵*ITAMP, Center for Astrophysics | Harvard & Smithsonian,
60 Garden St, Cambridge, Massachusetts 02138, USA*

We calculate, via variational techniques, single- and two-photon Rydberg microwave transitions, as well as scalar and tensor polarizabilities of sodium atom using the parametric one-electron valence potential, including the spin-orbit coupling. The trial function is expanded in a basis set of optimized Slater-type orbitals, resulting in highly accurate and converged eigen-energies up to $n = 60$. We focus our studies on the microwave band 90–150 GHz, due to its relevance to laser excitation in the Earth’s upper-atmospheric sodium layer for wavelength-dependent radiometry and polarimetry, as precise microwave polarimetry in this band is an important source of systematic uncertainty in searches for signatures of primordial gravitational waves within the anisotropic polarization pattern of photons from the cosmic microwave background. We present the most efficient transition coefficients in this range, as well as the scalar and tensor polarizabilities compared with available experimental and theoretical data.

I. INTRODUCTION

The frequency domain in the MHz–THz range is a preferred band for sensing and metrology in the radio to millimeter wavelengths, as well as for establishing measurement standards. One of the most promising and sensitive recent developments in this field is with the use of Rydberg atom electric field sensing [1–14]. This appealing aspect allows for amplitude sensing of RF fields [12] and for imaging with sub-wavelength spatial resolution [4, 11].

A major source of uncertainty in searches for signatures of primordial gravitational waves within the polarization pattern of the cosmic microwave background (CMB), and a source that is growing in relative importance as the precision of such searches improves, is the lack of microwave sources of precisely-known polarization in the sky to use for calibration [15]. Recently, excitations with lasers in the Earth’s sodium layer were shown to dramatically improve photometric systematics, via a laser photometric ratio star (LPRS) in the visible and near-infrared frequencies [16–18]. It may be possible to extend the LPRS to precise calibration of microwave telescopes, such as the BICEP/Keck Array, which measure the polarization anisotropy of the CMB, and future enlarged and improved microwave observatories such as CMB-S4 [19, 20]. Polarized microwave and millimeter-wave radiation from Rydberg excited atoms in the sodium layer could be used for precise relative radiometric and polarimetric calibrations of such ground-based microwave and millimeter-wave telescopes.

Precise measurements and calculations of atomic polarizability play an essential role not only in metrology but for quantum information processing, optical trapping and cooling, and interparticle collision studies. The Einstein A coefficients are especially required for applications in atmospheric physics and astrophysics. There is a great need to know these quantities with high accuracy over a wide range of frequencies.

The primary source of recommended data for atomic parameters of the sodium atom is the report of NIST [21, 22]. Kelleher and Podobedova [21] compiled frequencies and spontaneous emission coefficients (Einstein A coefficients) for transitions in Na up to $n = 11$ and angular momentum $0 \leq l \leq 3$. It is worth noting that Gallagher

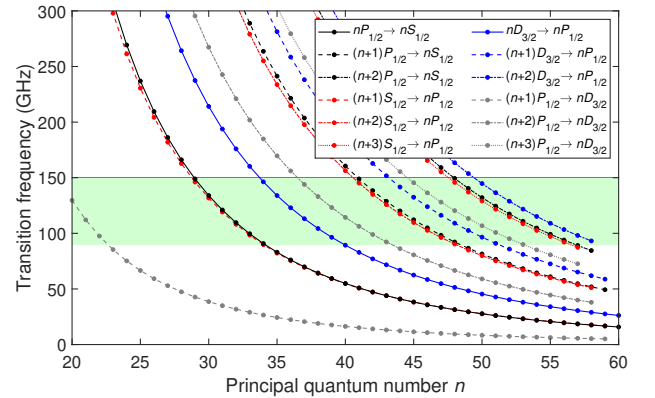


FIG. 1. The $nP_{1/2} \leftrightarrow n'S_{1/2}$ and $nD_{3/2} \leftrightarrow n'P_{1/2}$ electron transitions in the highly excited Na atom. The green area indicates the microwave frequency band of 90 to 150 GHz. The spectrum for the $nP_{3/2} \leftrightarrow n'S_{1/2}$ and $nD_{3/2,5/2} \leftrightarrow n'P_{3/2}$ electron transitions looks essentially the same.

* e-mail: teomar@chem.umk.pl

et al. [23] made radio-frequency resonance measurements of the nP and nD series for $n = 16$ –19 and $n = 15$ –17, respectively. Fabre, Haroche, and Goy [24] observed more highly excited states of Na and measured the microwave resonance frequencies between S , P , D , and F states for $n = 23$ –41 as well as the polarizabilities of nS and nP levels.

In this article, we extend the previous data on Einstein coefficients and scalar and tensor polarizabilities of Rydberg states of the sodium atom to include higher principal quantum numbers. Based on an accurate variational approach [25, 26], transition frequencies, spontaneous and stimulated emission coefficients, and polarizabilities for the Na($n \leq 60$, $l \leq 3$) atom are calculated. We particularly focus on the prominent lines in the 90–150 GHz range, of interest for precision microwave relative radiometric and polarimetric laser excitation of the sodium layer [16–18]. Rydberg transitions within Earth’s mesosphere can offer precise sources of relative radiometry and polarimetry in the microwave, with the use of free-space lasers [27]. The green area in Fig. 1 shows the microwave band under consideration within the calculated transition spectrum of Na. One can see the abundance of atomic electron transitions we will concentrate on in this article.

II. THEORY AND COMPUTATION

A. Hamiltonian terms

We consider a system comprised of the valence electron interacting with a closed alkali-metal positive-ion core. The Hamilton operator can be written as (in a.u.)

$$\hat{H} = -\frac{1}{2}\nabla^2 + V_l(r) + V_{LS}(r), \quad (1)$$

where $V_l(r)$ is the one-dimensional effective model potential [28] and $V_{LS}(r)$ is the spin-orbit coupling [29]. The form of $V_l(r)$ depends on the nuclear charge (Z) of the atom, five parameters ($a_k^{(l)}$, $k = 1, 2, 3, 4$, and $r_c^{(l)}$), and the static dipole polarizability (α_c) of the singly charged core,

$$V_l(r) = -\frac{1}{r} - \frac{(Z-1)}{r} \exp[-a_1^{(l)}r] + (a_3^{(l)} + a_4^{(l)}r) \exp[-a_2^{(l)}r] - \frac{\alpha_c}{2r^4} \left(1 - \exp\left[-\left(r/r_c^{(l)}\right)^6\right]\right). \quad (2)$$

All the parameters for the sodium atom are given in Ref. [28]. The spin-orbit interaction potential may be expressed as (in a.u.)

$$V_{LS}(r) = \mathbf{L} \cdot \mathbf{S} \frac{\alpha^2}{2} \frac{1}{r} \frac{dV_l(r)}{dr} \left(1 - \frac{\alpha^2}{2} V_l(r)\right)^{-2}, \quad (3)$$

where $(\mathbf{L} \cdot \mathbf{S}) = \frac{1}{2}[j(j+1) - l(l+1) - \frac{3}{4}]$ and α stands for the fine-structure constant. As usual, j and l are the

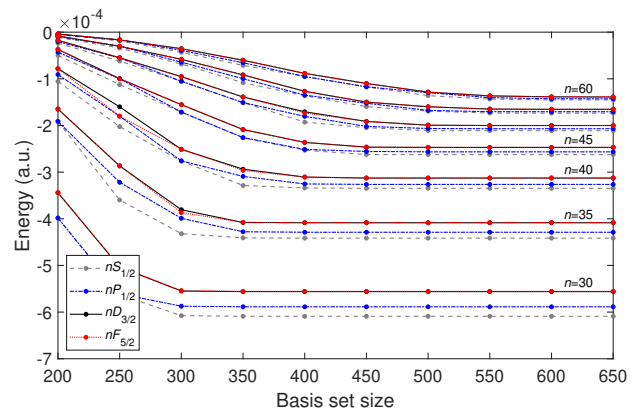


FIG. 2. Convergence of $nS_{1/2}$, $nP_{1/2}$, $nD_{3/2}$, and $nF_{5/2}$ energy levels with basis-set size, for different n .

total and orbital angular momentum quantum numbers, respectively, where $j = l \pm \frac{1}{2}$.

We compute the eigen-spectra of the time-independent Schrödinger equation with the Hamiltonian (1) for Na($l \leq 3$, j) by applying the Ritz variational method in a trial space spanned by 650 optimized Slater-type orbitals (STOs). Technical details of the calculations are described in sections II of Ref. [25] and II.B of Ref. [26]. The calculations are carried out in quadruple precision. According to the variational principle for excited states, the lowest k -th eigen-energy (E_k) is the upper bound for the respective exact energy of the k -th state of Na. Any increase in the size of the basis set gives an improved approximation (i.e., lower energy) E_k for the k -th exact energy level. The convergence of selected energies with respect to the size of the basis set is displayed in Fig. 2. Saturation of the obtained results is visible when the trial space is enlarged. However, the higher the energy level, the slower convergence to the exact solution. The variational method with 650 STOs enables us to compute the energy spectrum for any (l, j) series up to $n = 60$ with accuracy not less than four significant digits (for the worst case), and the accuracy increases with decreasing n .

B. Polarizabilities

The polarizability of an atom is a measure of the atomic orbital distortion, exposed to an applied electric field. In the case of linearly polarized electric field F , the interaction with an atom in a state described by the quantum numbers j (total angular momentum) and m_j (the projection of j on the axis of propagation of the electromagnetic wave) is written as [30]

$$V_F = -\frac{1}{2} \left(\alpha_0 + \alpha_2 \frac{3m_j^2 - j(j+1)}{j(2j-1)} \right) F^2. \quad (4)$$

TABLE I. The convergence of the scalar and tensor polarizabilities (in a.u.), for the lowest states and some of the sodium Rydberg states with respect to n' , in the sums of Eqs. (5) and (6). The notation (x) denotes $\times 10^x$. The closed interval $[a, b]$ is defined by $\{n' \in \mathbb{N} : a \leq n' \leq b\}$.

n	n'	$\alpha_0(S_{1/2})$	$\alpha_0(P_{3/2})$	$\alpha_0(D_{5/2})$	$\alpha_2(P_{3/2})$	$\alpha_2(D_{5/2})$
3	≤ 60	1.66919(2)	3.56032(2)	6.38605(3)	-8.45922(1)	-5.07481(3)
	≤ 50	1.66919(2)	3.56023(2)	6.38596(3)	-8.45900(1)	-5.07478(3)
	≤ 40	1.66919(2)	3.56005(2)	6.38580(3)	-8.45859(1)	-5.07474(3)
	≤ 30	1.66919(2)	3.55966(2)	6.38544(3)	-8.45768(1)	-5.07463(3)
	≤ 20	1.66918(2)	3.55853(2)	6.38439(3)	-8.45501(1)	-5.07434(3)
	≤ 10	1.66914(2)	3.55191(2)	6.37784(3)	-8.43823(1)	-5.07246(3)
30	≤ 60	6.78051(9)	-9.70554(10)	1.62196(12)	9.81951(9)	-5.16578(11)
	≤ 50	6.78048(9)	-9.70555(10)	1.62196(12)	9.81954(9)	-5.16578(11)
	≤ 40	6.78031(9)	-9.70562(10)	1.62196(12)	9.81972(9)	-5.16578(11)
	≤ 35	6.77951(9)	-9.70593(10)	1.62196(12)	9.82066(9)	-5.16576(11)
	[10, 60]	6.78051(9)	-9.70554(10)	1.62196(12)	9.81951(9)	-5.16578(11)
	[20, 60]	6.78052(9)	-9.70554(10)	1.62196(12)	9.81951(9)	-5.16578(11)
50	≤ 60	1.94641(11)	-3.85495(12)	5.82569(13)	3.98254(11)	-1.85504(13)
	≤ 55	1.94615(11)	-3.85504(12)	5.82568(13)	3.98282(11)	-1.85503(13)
	[10, 60]	1.94641(11)	-3.85495(12)	5.82569(13)	3.98254(11)	-1.85504(13)
	[20, 60]	1.94641(11)	-3.85495(12)	5.82569(13)	3.98254(11)	-1.85504(13)
	[30, 60]	1.94641(11)	-3.85495(12)	5.82569(13)	3.98254(11)	-1.85504(13)
	[40, 60]	1.94642(11)	-3.85495(12)	5.82569(13)	3.98254(11)	-1.85504(13)
[45, 60]	1.94665(11)	-3.85494(12)	5.82570(13)	3.98250(11)	-1.85504(13)	

We calculate the scalar and tensor polarizabilities, a_0 and a_2 , respectively, of $\text{Na}(n, l, j)$ states as follows [31, 32]

$$a_0 = -\frac{2}{3} \sum_{n', l', j'} (2j' + 1) \left\{ \begin{matrix} l & j & 1/2 \\ j' & l' & 1 \end{matrix} \right\}^2 \times \max(l, l') \frac{|\langle nl|r|n'l' \rangle|^2}{E_{n,l,j} - E_{n',l',j'}}, \quad (5)$$

$$a_2 = -2 \left[\frac{10j(2j-1)(2j+1)}{3(j+1)(2j+3)} \right]^{1/2} \sum_{n', l', j'} (-1)^{j+j'} (2j' + 1) \times \max(l, l') \left\{ \begin{matrix} l & j & 1/2 \\ j' & l' & 1 \end{matrix} \right\}^2 \left\{ \begin{matrix} j & j' & 1 \\ 1 & 2 & j \end{matrix} \right\} \frac{|\langle nl|r|n'l' \rangle|^2}{E_{n,l,j} - E_{n',l',j'}}. \quad (6)$$

The curly brackets, $\{ \dots \}$, refer to a Wigner $6j$ symbol. In theory, the summations should be carried out over all bound and continuum states, but in practice, only the neighboring states contribute significantly [32]. Obviously, the dipole-allowed transitions are for $l' = l \pm 1$. Since we successfully calculated the $\text{Na}(nS_{1/2}, nP_{1/2,3/2}, nD_{3/2,5/2}, nF_{5/2,7/2})$ energy levels up to $n = 60$, we were able to determine the polarizabilities for $nS_{1/2}, nP_{1/2,3/2}$, and $nD_{3/2,5/2}$ series with $n \leq 58$ with high accuracy. Note that the radial dipole matrix elements, $\langle nl|r|n'l' \rangle$, do not depend on j , i.e., the wave functions describe the (n, l) states, where spin-orbit coupling is not incorporated. In turn, energy levels in the above equations include the fine-structure splitting due to the spin-orbit

interaction.

The quality of the polarizability computations in the range we are interested in is quite satisfactory. Table I shows convergence of polarizabilities with respect to the number of terms in evaluating Eqs. (5) and (6) for selected states. It is plainly seen that the polarizabilities are contributed by the most adjacent intermediate states. Let us take a closer look at the results for $\alpha_0(P_{3/2})$ as an example. The scalar polarizability for $3P_{3/2}$ is equal to 355.191 a.u. when the summation in Eq. (5) is over neighboring states ($n' \leq 10$), and 356.032 a.u. when more states are taken into account ($n' \leq 60$). The relative error is less than 0.24%. Moreover, one can see in Table I how the results saturate when the upper limit of the summation systematically increases (from 10 to 60 with step 10). The convergence of the scalar polarizability for excited states is even better. The relative error of $\alpha_0(50P_{3/2})$ when $45 \leq n' \leq 60$ compared to the case with $n' \leq 60$ is less than 0.0003%. Similar observations can be made for other polarizabilities presented in Table I.

C. Einstein coefficients

The Einstein coefficients for atom-photon reactions are intrinsic properties of any atom that do not depend on the nature of the external electromagnetic radiation.

The Einstein A coefficient corresponds to the rate of spontaneous emission from a higher energy state (k) to

a lower energy state (i), $A_{k,i} \equiv A[(n, l, j) \rightarrow (n', l', j')]$. Using this notation, we have (in a.u.) [33]

$$A_{k,i} = \frac{4}{3(2j+1)} \alpha^3 E_{k,i}^3 |\langle nlj || D(r) || n'l'j' \rangle|^2, \quad (7)$$

where $E_{k,i}$ is the energy of the transition, $E_{k,i} = E_k - E_i = E_{n,l,j} - E_{n',l',j'} = \hbar\omega_{k,i}$. The square of the matrix element of the transition dipole operator, $D(r)$, is given by [33, 34]

$$|\langle nlj || D(r) || n'l'j' \rangle|^2 = (2j+1)(2j'+1) \left\{ \begin{matrix} l & j & 1/2 \\ j' & l' & 1 \end{matrix} \right\}^2 \times \max(l, l') |\langle nl|r|n'l' \rangle|^2. \quad (8)$$

The Einstein B coefficient describes the rate of stimulated emission and absorption per time and energy density of the incident radiation. Stimulated emission can be related to spontaneous emission by the inverse cube of the transition frequency from the initial (upper) to the final (lower) state by (in a.u.) [35, 36]

$$B_{k,i} = \frac{c^3 \pi^2}{\omega_{k,i}^3} A_{k,i}. \quad (9)$$

Incorporating Eqs. (7) and (8) into Eq. (9), we get a final equation for $B_{k,i}$, which does not depend directly on the energy level difference (in a.u.)

$$B_{k,i} = \frac{4}{3} \pi^2 (2j'+1) \left\{ \begin{matrix} l & j & 1/2 \\ j' & l' & 1 \end{matrix} \right\}^2 \times \max(l, l') |\langle nl|r|n'l' \rangle|^2. \quad (10)$$

The stimulated absorption rate coefficient, $B_{i,k}$, is proportional to $B_{k,i}$ by the ratio of the statistical weights [35, 36],

$$B_{i,k} = \frac{g_k}{g_i} B_{k,i}. \quad (11)$$

D. Two-photon transitions

The probability per second to emit two photons, one at frequency ω_1 and the other at ω_2 , in the transition $nS_{1/2} \rightarrow n'P_{j'} \rightarrow n''S_{1/2}$, $j' = \frac{1}{2}, \frac{3}{2}$, is (in a.u.) [37–39]

$$A(y)dy = \frac{8}{27\pi} \alpha^6 \omega_{n,n''}^7 y^3 (1-y)^3 |M_{j'}|^2 dy, \quad (12)$$

where $y = \omega_1/\omega_{n,n''}$, $\omega_{n,n''} = \omega_1 + \omega_2$, and

$$M_{j'} = M_{j'}^{(1)} + M_{j'}^{(2)} = \sum_{n'} \langle nS|r|n'P \rangle \langle n'P|r|n''S \rangle \times \left(\frac{1}{E_{n'P_{j'}} - E_{nS_{1/2}} + y(E_{nS_{1/2}} - E_{n''S_{1/2}})} + \frac{1}{E_{n'P_{j'}} - E_{nS_{1/2}} + (1-y)(E_{nS_{1/2}} - E_{n''S_{1/2}})} \right). \quad (13)$$

In the above, $\hbar\omega_{n,n''}$ is the transition energy from an upper state (n, l, j) to a lower state (n'', l'', j'') , $E_{n,l,j} - E_{n'',l'',j''}$, and the sum is performed over all intermediate dipole-allowed atomic states n' .

The total probability for the two-photon emission is

$$A_t = \frac{1}{2} \int_0^1 A(y) dy. \quad (14)$$

The factor in front of the integral avoids double counting of photons. Consequently, the mean life time is $\tau = A_t^{-1}$.

III. RESULTS AND DISCUSSION

A. Rydberg energy levels

We calculate the energy levels for the $nS_{1/2}$, $nP_{1/2}$, $nP_{3/2}$, $nD_{3/2}$, $nD_{5/2}$, $nF_{5/2}$, and $nF_{7/2}$ series for $n \leq 60$. Fig. 1 presents energy level differences between two states in the 0–300 GHz range as a function of the principal quantum number. The green area marks the 90–150 GHz microwave band. It is easy to determine between which two adjacent Rydberg states there is an atomic electron Rydberg transition in a specific frequency range; for example, the transition frequency of $nP_{1/2} \rightarrow nS_{1/2}$ is about 150 GHz for $n = 29$ and 90 GHz for $n = 34$. Fig. 1 reveals that, in general, the one-photon transition for $|n - n'| \leq 2$ within the microwave band occurs when the principal quantum number is less than 60.

B. Static polarizabilities of Rydberg states

The scalar and tensor polarizabilities for excited states of Na, an excellent test of the quality of the eigenfunctions and eigenvalues, are presented in Table II. The results are in good accord with theoretical [23, 24, 40–42, 44, 47, 48] as well as experimental [23, 24, 43, 45–48] findings. Although our basis set was optimized for excited energy levels, the calculated values for the lower lying levels are in good agreement with the observed values. Several different techniques have been employed to determine α_0 and α_2 for the ground state and the first low-lying S , P , and D states; for example, Maroulis [40] used the coupled cluster method with singles, doubles, and perturbative triples (CCSD(T)), whereas Zhu *et al.* [44] applied relativistic many-body perturbation theory. Kamenski and Ovsiannikov [42] performed numerical computations with the Fues' model potential. In turn, Zhang and Mitroy [41] combined the non-relativistic configuration interaction technique with the semiempirical core potential. The reference measurement of the ground-state polarizability of Na was done with an atom interferometer by Pritchard and coworkers [43]. Our value of $\alpha_0(S_{1/2})$ is in agreement to better than $\pm 3\%$ with the experimental finding and better than $\pm 1\%$ with the results of Maroulis [40], and of Kamenski and Ovsiannikov [42]. It is interesting to point out that $\alpha_2(P_{3/2})$

TABLE II. Selected scalar (given by α_0) and tensor (given by α_2) polarizabilities of the nS , nP , and nD states of Na in a.u. The notation (x) denotes $\times 10^x$.

n	$\alpha_0(S_{1/2})$	$\alpha_0(P_{1/2})$	$\alpha_0(P_{3/2})$	$\alpha_0(D_{3/2})$	$\alpha_0(D_{5/2})$	$\alpha_2(P_{3/2})$	$\alpha_2(D_{3/2})$	$\alpha_2(D_{5/2})$
3	1.669(2)	3.556(2)	3.560(2)	6.399(3)	6.386(3)	-8.459(1)	-3.565(3)	-5.075(3)
	1.655(2) ^a	3.607(2) ^b		6.396(3) ^b		-8.789(1) ^b		-5.073(3) ^b
	1.673(2) ^c	3.449(2) ^c	3.462(2) ^c	6.646(3) ^c	6.622(3) ^c	-9.966(1) ^c	-3.723(3) ^c	-5.285(3) ^c
	1.627(2) ^d	3.597(2) ^e	3.614(2) ^e			-8.80(1) ^e		
	1.59(2) ^f	3.49(2) ^g				-1.13(2) ^g		
4	3.132(3)	-4.517(3)	-4.486(3)	6.112(5)	6.113(5)	-1.361(2)	-1.443(5)	-2.060(5)
	3.309(3) ^c	-4.694(3) ^c	-4.628(3) ^c	6.365(5) ^c	6.358(5) ^c	-3.565(2) ^c	-1.501(5) ^c	-2.140(5) ^c
	3.110(3) ^b			6.109(5) ^h	6.107(5) ^h		-1.432(5) ^h	-2.052(5) ^h
				6.241(5) ⁱ	6.273(5) ⁱ		-1.547(5) ⁱ	-2.138(5) ⁱ
5	2.191(4)	-5.867(4)	-5.839(4)	4.009(6)	4.010(6)	2.674(3)	-9.174(5)	-1.310(6)
	2.352(4) ^c	-5.990(4) ^c	-5.933(4) ^c	4.065(6) ^c	4.060(6) ^c	1.387(3) ^c	-9.317(5) ^c	-1.328(6) ^c
	2.33(4) ^h							
	2.1(4) ⁱ							
10	4.137(6)	-2.476(7)	-2.467(7)	6.900(8)	6.902(8)	2.167(6)	-1.545(8)	-2.207(8)
								-2.1(8) ^j
								-2.8(8) ^k
11	8.069(6)	-5.262(7)	-5.243(7)	1.364(9)	1.365(9)	4.719(6)	-3.053(8)	-4.360(8)
								-4.22(8) ^j
								-4.82(8) ^k
12	1.475(7)	-1.038(8)	-1.034(8)	2.536(9)	2.537(9)	9.486(6)	-5.671(8)	-8.099(8)
								-7.84(8) ^j
								-8.24(8) ^k
15	6.767(7)	-5.749(8)	-5.728(8)	1.234(10)	1.234(10)	5.451(7)	-2.756(9)	-3.936(9)
				1.19(10) ^l				-3.8(9) ^l
								-4.26(9) ^m
16	1.046(8)	-9.367(8)	-9.333(8)	1.947(10)	1.948(10)	8.958(7)	-4.348(9)	-6.210(9)
		-9.00(8) ^l		1.89(10) ^l		7.96(7) ^l		-5.99(9) ^l
						8.8(7) ^m		-5.91(9) ^m
17	1.572(8)	-1.478(9)	-1.473(9)	2.987(10)	2.988(10)	1.424(8)	-6.669(9)	-9.524(9)
		-1.40(9) ^l		2.88(10) ^l		1.26(8) ^l		-9.20(9) ^l
						1.3(8) ^m		-1.12(10) ^m
18	2.305(8)	-2.268(9)	-2.260(9)	4.470(10)	4.471(10)	2.198(8)	-9.978(9)	-1.425(10)
		-2.18(9) ^l				1.97(8) ^l		
						2.0(8) ^m		
19	3.307(8)	-3.394(9)	-3.382(9)	6.543(10)	6.544(10)	3.309(8)	-1.460(10)	-2.085(10)
		-3.25(9) ^l				2.98(8) ^l		
						3.0(8) ^m		
20	4.653(8)	-4.969(9)	-4.952(9)	9.389(10)	9.391(10)	4.868(8)	-2.095(10)	-2.992(10)
23	1.176(9)	-1.396(10)	-1.391(10)	2.509(11)	2.510(11)	1.383(9)	-5.599(10)	-7.996(10)
	(*)	-1.4(10) ⁿ				1.4(9) ⁿ		
	(**)	-1.7(10) ^o				1.8(9) ^o		
24	1.558(9)	-1.908(10)	-1.902(10)	3.384(11)	3.385(11)	1.897(9)	-7.551(10)	-1.078(11)
25	2.040(9)	-2.575(10)	-2.566(10)	4.509(11)	4.509(11)	2.567(9)	-1.006(11)	-1.436(11)
30	6.781(9)	-9.740(10)	-9.706(10)	1.622(12)	1.622(12)	9.820(9)	-3.617(11)	-5.166(11)
32	1.036(10)	-1.556(11)	-1.551(11)	2.550(12)	2.551(12)	1.574(10)	-5.689(11)	-8.124(11)
		-1.6(11) ⁿ				1.6(10) ⁿ		
		-1.55(11) ^o				1.5(10) ^o		
34	1.544(10)	-2.414(11)	-2.406(11)	3.902(12)	3.903(12)	2.449(10)	-8.703(11)	-1.243(12)
		-2.6(11) ⁿ				2.6(10) ⁿ		
		-3.03(11) ^o				3.3(10) ^o		
35	1.868(10)	-2.977(11)	-2.967(11)	4.782(12)	4.782(12)	3.024(10)	-1.066(12)	-1.523(12)
40	4.490(10)	-7.799(11)	-7.772(11)	1.219(13)	1.220(13)	7.968(10)	-2.720(12)	-3.884(12)
41	5.281(10)	-9.316(11)	-9.283(11)	1.450(13)	1.450(13)	9.527(10)	-3.233(12)	-4.618(12)
		-1.05(12) ⁿ						
		-1.31(12) ^o						
45	9.735(10)	-1.818(12)	-1.812(12)	2.784(13)	2.784(13)	1.866(11)	-6.208(12)	-8.866(12)
50	1.946(11)	-3.869(12)	-3.855(12)	5.824(13)	5.826(13)	3.983(11)	-1.299(13)	-1.855(13)
55	3.645(11)	-7.647(12)	-7.620(12)	1.136(14)	1.136(14)	7.894(11)	-2.533(13)	-3.617(13)

(*) $\alpha_0(24S_{1/2}) - \alpha_0(23S_{1/2}) = 0.37(9)$ Ref. [24] (theo.); (**) $\alpha_0(24S_{1/2}) - \alpha_0(23S_{1/2}) = 0.40(9)$ Ref. [24] (exp.);
^aRef. [40]; ^bRef. [41]; ^cRef. [42]; ^dRef. [43]; ^eRef. [44]; ^fRef. [45]; ^gRef. [46]; ^hRef. [47] (theo.); ⁱRef. [47] (exp.);
^jRef. [48] (theo.); ^kRef. [48] (exp.); ^lRef. [23] (theo.); ^mRef. [23] (exp.); ⁿRef. [24] (theo.); ^oRef. [24] (exp.)

TABLE III. Determined expansion coefficients of Eq. (15) for the scalar and tensor polarizabilities of low- and high-lying states of Na. The notation (x) denotes $\times 10^x$.

$\alpha_{0,2}^{(n,l,j)}$	$A_{0,2}^{(l,j)}$	$B_{0,2}^{(l,j)}$	$C_{0,2}^{(l,j)}$	$\delta_{0,2}^{(l,j)}$
$\alpha_0(nS_{1/2})$	1.21500(-1)	7.26440(1)	4.30899(1)	1.43461
$\alpha_0(nP_{1/2})$	-5.77239	-4.09439	3.53175	4.87711(-1)
$\alpha_0(nP_{3/2})$	-5.75251	-2.45217	-9.71749(-1)	7.22962(-1)
$\alpha_2(nP_{3/2})$	6.11501(-1)	7.99240	2.26122(1)	2.40946
$\alpha_0(nD_{3/2})$	7.47735(1)	7.89515	1.92152(1)	1.12710
$\alpha_2(nD_{3/2})$	-1.66751(1)	7.56835(-2)	-7.35366	1.07230(-2)
$\alpha_0(nD_{5/2})$	7.47878(1)	-6.94563	1.30233(1)	-9.93368(-1)
$\alpha_2(nD_{5/2})$	-2.38141(1)	9.20926(-2)	-7.36304	1.30110(-2)

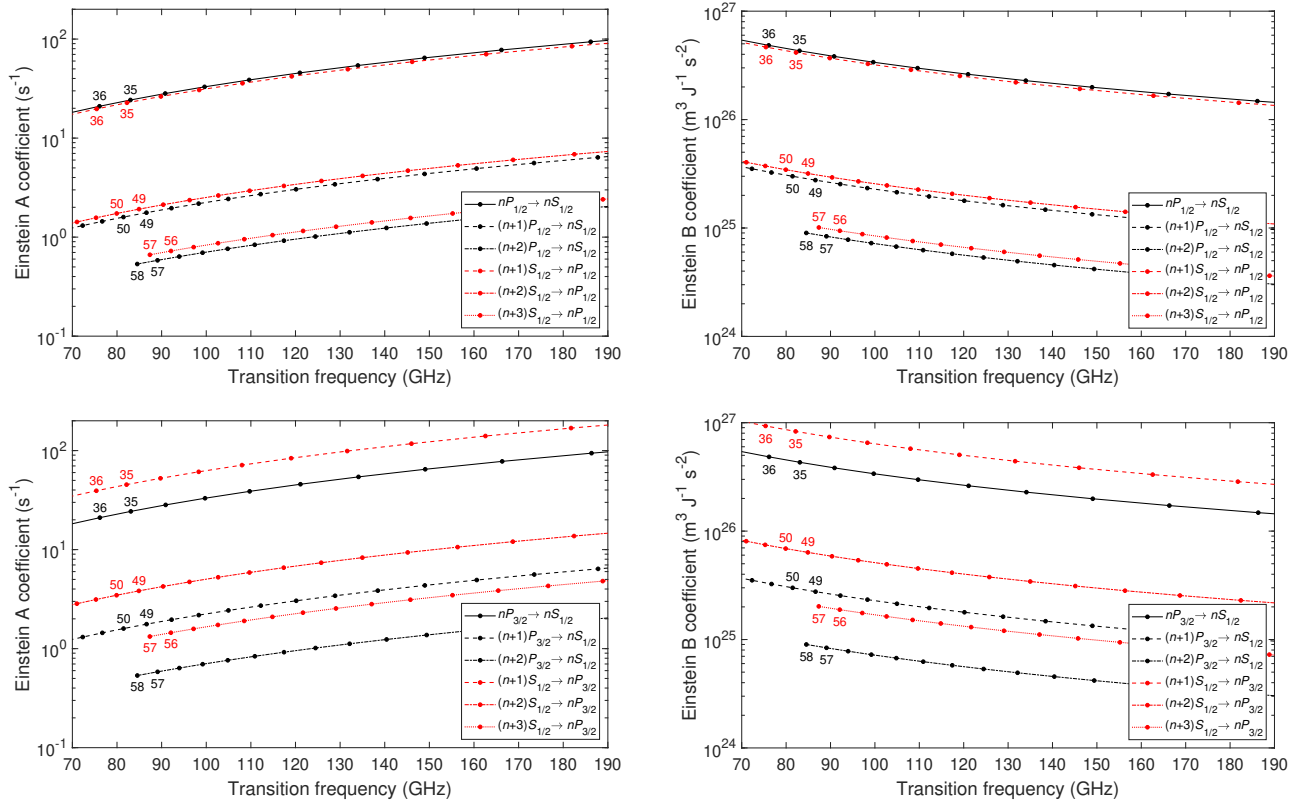


FIG. 3. The largest Einstein A (left panels) and B (right panels) coefficients for the $nP_{1/2} \leftrightarrow n'S_{1/2}$ (upper panels) and $nP_{3/2} \leftrightarrow n'S_{1/2}$ (lower panels) microwave transitions among highly excited states in sodium. Each point correlates to a specific principal quantum number, provided for some of the transitions noted in the legends.

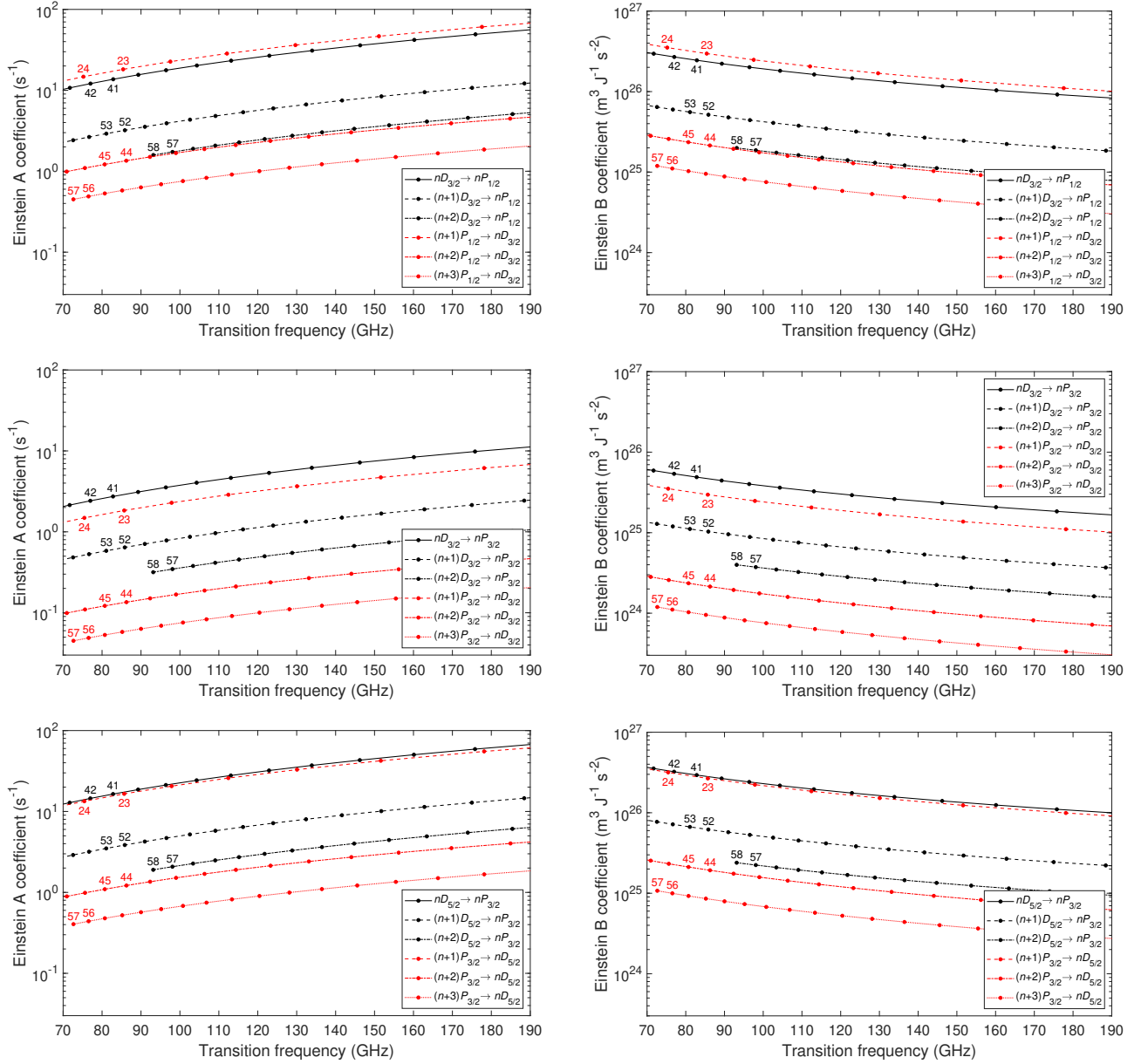


FIG. 4. The largest Einstein A (left panels) and B (right panels) coefficients for the $nD_{3/2} \leftrightarrow n'P_{1/2}$ (upper panels), $nD_{3/2} \leftrightarrow n'P_{3/2}$ (middle panels), and $nD_{5/2} \leftrightarrow n'P_{3/2}$ (lower panels) microwave transitions among highly excited states in sodium. Each point correlates to a specific principal quantum number, provided for some of the transitions noted in the legends.

for $n = 4$, determined by the two latter authors, differs significantly from the result presented here by more than a factor of two. Moreover, all the values of Kamenski and Ovsianikov [42] for $\alpha_2(P_{3/2})$ appear to be underestimated. A less accurate experimental result for $\alpha_0(S_{1/2})$ comes from the work of Molof *et al.* [45] using the E - H -gradient balance technique. In this case, the deviation is less than $\pm 5\%$.

The typical experimental determination of polarizability is with Stark shift measurements of resonance transitions. However, the number of measurements for highly

excited Rydberg states is relatively scarce. We contrasted our results with those of Fabre and Haroche [48] for $n = 10$ –12, Gallagher *et al.* [23] for $n = 15$ –19, and Fabre *et al.* [24] for $n = 23$ –41. When a weak electric field is applied, the tensor polarizability of an atom with one valence electron can be effectively obtained from the difference in polarizabilities between two proper magnetic sublevels. Assuming that the fine-structure splitting is small in comparison to the energy distance for $l = l' \pm 1$, Eqs. (5) and (6) simplify, which consequently leads to $\alpha_0(P_{1/2}) = \alpha_0(P_{3/2})$, $\alpha_0(D_{3/2}) = \alpha_0(D_{5/2})$, and

$\alpha_2(D_{3/2}) = \frac{7}{10}\alpha_2(D_{5/2})$. Note that $\alpha_2(P_{1/2})$ is always equal to zero. Our results show that this is quite a reasonable approximation for the sodium atom, especially for the highly excited states. A smaller, but still significant, difference between $\alpha_2(F_{5/2})$ and $\alpha_2(F_{7/2})$ also exists. This is because the spin-orbit splitting decreases with increasing l . Based on the above mentioned approximation, $\alpha_2(F_{5/2})$ will be equal to $\frac{6}{7}\alpha_2(F_{7/2})$. One can see in Table II, the striking agreement between our scalar and tensor polarizabilities for $n = 32$ with the experimental values of Fabre *et al.* [24]. The agreement is less impressive for higher excited states ($n = 34$ and $n = 41$). The polarizabilities were also determined theoretically, based on the Coulomb approximation for those states in Ref. [24].

The Rydberg polarizabilities scale as n^7 [49]. To cover the entire space of bound states with the values of α_0 and α_2 for the sodium atom, we may expand the polarizability in terms of a power series of the effective principal quantum number $n^* = n - \delta^{(l,j)}$, where $\delta^{(l,j)}$ is the quantum defect, as follows

$$\alpha_{0,2}^{(n,l,j)} = A_{0,2}^{(l,j)} \left(n - \delta_{0,2}^{(l,j)} \right)^7 \times \left(1 + \frac{B_{0,2}^{(l,j)}}{n - \delta_{0,2}^{(l,j)}} + \frac{C_{0,2}^{(l,j)}}{\left(n - \delta_{0,2}^{(l,j)} \right)^2} + \dots \right). \quad (15)$$

The fitted coefficients $A_{0,2}^{(l,j)}$, $B_{0,2}^{(l,j)}$, $C_{0,2}^{(l,j)}$, and $\delta_{0,2}^{(l,j)}$ of calculated α_0 and α_2 with the above expression, are presented in Table III for the $S_{1/2}$, $P_{1/2,3/2}$, and $D_{3/2,5/2}$ states. The goodness of the fits is excellent. The three-term expansion (15) with the coefficients, Table III, reproduces the scalar and tensor polarizabilities to four significant figures, as shown in Table II.

C. Einstein A & B coefficients

We determined the Einstein coefficients of the $nP_{1/2,3/2} \leftrightarrow n'S_{1/2}$ and $nD_{3/2,5/2} \leftrightarrow n'P_{1/2,3/2}$ microwave emissions in the sodium Rydberg series. The upper left panel of Fig. 3 presents the results of the A coefficients for the $nP_{1/2} \rightarrow nS_{1/2}$, $(n+1)P_{1/2} \rightarrow nS_{1/2}$, $(n+2)P_{1/2} \rightarrow nS_{1/2}$, $(n+1)S_{1/2} \rightarrow nP_{1/2}$, $(n+2)S_{1/2} \rightarrow nP_{1/2}$, and $(n+3)S_{1/2} \rightarrow nP_{1/2}$ transitions in the 70–190 GHz frequency range. The two most dominant A coefficients are for the $nP_{1/2} \rightarrow nS_{1/2}$ and $(n+1)S_{1/2} \rightarrow nP_{1/2}$ one-photon decay, with $n = 34$ at about 90 GHz and $n = 29$ at about 150 GHz. The lower left panel of Fig. 3 is for transitions emanating from and to $P_{3/2}$. It is worth noting that the A coefficient is about two times larger for $nS_{1/2} \rightarrow n'P_{3/2}$ than for $nS_{1/2} \rightarrow n'P_{1/2}$. The ratio $\frac{A(nS_{1/2} \rightarrow n'P_{3/2})}{A(nS_{1/2} \rightarrow n'P_{1/2})} = 2$, but only when one assumes $E_{n'P_{1/2}} = E_{n'P_{3/2}}$, i.e., when spin-orbit coupling is neglected.

TABLE IV. Einstein A coefficients (10^5 s^{-1}) for spontaneous emission to the $\text{Na}(3P_{3/2})$ state.

n	$nS_{1/2} \rightarrow 3P_{3/2}$		$nD_{3/2} \rightarrow 3P_{3/2}$	
	Other works	This work	Other works	This work
3			85.76 ^a 84.95 ^b 85.7 ^c	85.59
4	178.0 ^a 176 ^c	175.0	20.23 ^a 20.15 ^b 20.2 ^c	20.50
5	50.75 ^a 49.8 ^c	49.50	8.147 ^a 8.109 ^b 8.15 ^c	8.298
6	23.15 ^a 22.7 ^c	22.51	4.159 ^a 4.129 ^b 4.14 ^c	4.244
7	12.63 ^a 12.3 ^c	12.24	2.429 ^a 2.44 ^c	2.484
8	7.662 ^a 7.50 ^c	7.414	1.550 ^a 1.95 ^c	1.587
9	5.000 ^a 5.61 ^c	4.834	1.141 ^a	1.079
10	3.444 ^a 6.50 ^c	3.328	0.7498 ^a	0.7688
11	2.473 ^a	2.390	0.5535 ^a	0.5678
12	1.836 ^a	1.774	0.4200 ^a	0.4317
13	1.401 ^a	1.353	0.3262 ^a	0.3362
14	1.094 ^a	1.055	0.2587 ^a	0.2670
15	0.8700 ^a	0.8391	0.2088 ^a	0.2157
16	0.7032 ^a	0.6782	0.1710 ^a	0.1768
17	0.5764 ^a	0.5560	0.1418 ^a	0.1467
18	0.4783 ^a	0.4615	0.1189 ^a	0.1231
19	0.4012 ^a	0.3872	0.1008 ^a	0.1044
20	0.3398 ^a	0.3281	0.08616 ^a	0.08925
21	0.2904 ^a	0.2804	0.07426 ^a	0.07692
22	0.2500 ^a	0.2416	0.06446 ^a	0.06677
23	0.2169 ^a	0.2096	0.05630 ^a	0.05833
24	0.1894 ^a	0.1830	0.04946 ^a	0.05126
25	0.1663 ^a	0.1607	0.04369 ^a	0.04529
26	0.1469 ^a	0.1419	0.03879 ^a	0.04021
27	0.1304 ^a	0.1259	0.03459 ^a	0.03587
28	0.1162 ^a	0.1123	0.03098 ^a	0.03213
29	0.1041 ^a	0.1005	0.02786 ^a	0.02889
30	0.09356 ^a	0.09035	0.02514 ^a	0.02608
35	0.05775 ^a	0.05574	0.01578 ^a	0.01637
40	0.03811 ^a	0.03678	0.01055 ^a	0.01095
45	0.02646 ^a	0.02553	0.007402 ^a	0.007678
50	0.01911 ^a	0.01844	0.005392 ^a	0.005592
55		0.01375		0.004198
60		0.01052		0.003223

^aRef. [33]; ^bRef. [50] (taken from Ref. [33]); ^cRef. [21]

Fig. 4 shows the Einstein A coefficients for the $nD_{3/2} \leftrightarrow n'P_{1/2}$ (upper left panel), $nD_{3/2} \leftrightarrow n'P_{3/2}$ (middle left panel), and $nD_{5/2} \leftrightarrow n'P_{3/2}$ (lower left panel) microwave transitions, where $|n - n'| \leq 3$. Figures 3 and 4 allow an easy reading between exactly which states the transition occurs at a given frequency — each point corresponds to a specific n . The largest A coefficient among those investigated here is for the

TABLE V. Lifetimes (in μs) of sodium Rydberg states, compared with low-temperature measurements.

n	$nS_{1/2}$	$nD_{3/2}$	$nD_{5/2}$
17	5.203	4.508	4.512
		4.46 ^a	
18	6.263	5.351	5.356
		5.75 ^a	
19	7.459	6.294	6.299
	7.42 ^a	6.90 ^a	
20	8.800	7.340	7.346
	8.9 ^a	7.7 ^a	
21	10.29	8.496	8.503
	11.3 ^a	8.6 ^a	
22	11.94	9.768	9.776
	12.2 ^a	10.2 ^a	
23	13.76	11.16	11.17
	14.5 ^a	11.4 ^a	
24	15.76	12.68	12.69
	16.6 ^a	13.9 ^a	
25	17.94	14.33	14.34
	18.6 ^a	15.0 ^a	
26	20.32	16.12	16.13
	21.2 ^a	16.9 ^a	
27	22.89	18.05	18.06
	23.8 ^a	17.7 ^a	
28	25.67	20.12	20.14
	24.9 ^a		

^aRef. [51]

$(n+1)S_{1/2} \rightarrow nP_{3/2}$ decay. An analogous situation occurs for the B coefficients, which are displayed in the right panels in Figs. 3 and 4. It should be noted that as the frequency increases, each of the curves for the B coefficients tends to trend lower.

The A coefficients for spontaneous emission from the low- and high-lying $nS_{1/2}$ and $nD_{3/2}$ energy levels, where $n \leq 60$, to the lowest $P_{3/2}$ state are presented in Table IV. They are compared with theoretical results of Miculis and Meyer [33] and the available NIST data [21]. The agreement is excellent. Note that the report of Kelleher and Podobedova from NIST [21] contains data for transitions from low-excited states only. We would like to point out one particular transition in the NIST report, i.e., the $10S_{1/2} \rightarrow 3P_{3/2}$ transition. It is almost double our result as well as the transition of Miculis and Meyer [33].

Additionally, we determined the radiative lifetimes of the sodium $nS_{1/2}$ and $nD_{3/2,5/2}$ states for $n = 17$ –28 and compared them directly with low-temperature measurements of Spencer *et al.* [51]. The lifetime (τ_k) against spontaneous emission of the upper state (k) is related to the sum of such Einstein $A_{k,i}$ coefficients over all allowed transitions to lower states, $\tau_k^{-1} = \sum_i A_{k,i}$. Since the experiment was carried out in a cooled environment, the effect of blackbody-induced transfer can be neglected in the theoretical considerations. Our results and the experimental values are presented in Table V. One may notice the measurement data exhibit less smooth behavior than the computed values; however, the agreement

between the results is good. The lifetime increases with increasing n , varying between 4 and 26 μs .

D. Two-photon transitions

Dyubko and coworkers [52] measured the frequency of the two-photon transition $\text{Na}(29S_{1/2} \rightarrow 30S_{1/2})$ and obtained a value of 2×147542 MHz. Our calculated value is 2×147528 MHz, helping to validate the accuracy of our results. The fractional difference is less than 0.01%.

We calculated the full two-photon emission spectra for transitions $35S_{1/2}$ to $34S_{1/2}$ and $30S_{1/2}$ to $29S_{1/2}$ via $n'P_{j'}$. The choice was dictated by the fact that $E_{35S_{1/2}} - E_{34S_{1/2}} = 181$ GHz ($\approx 2 \times 90$ GHz) and $E_{30S_{1/2}} - E_{29S_{1/2}} = 295$ GHz ($\approx 2 \times 150$ GHz); moreover, as we mentioned earlier, the highest values for the one-photon emission probabilities are for the $nP_j \rightarrow nS_{1/2}$ and $(n+1)S_{1/2} \rightarrow nP_{j'}$ transitions. The results are presented in Fig. 5. The black and red curves show the

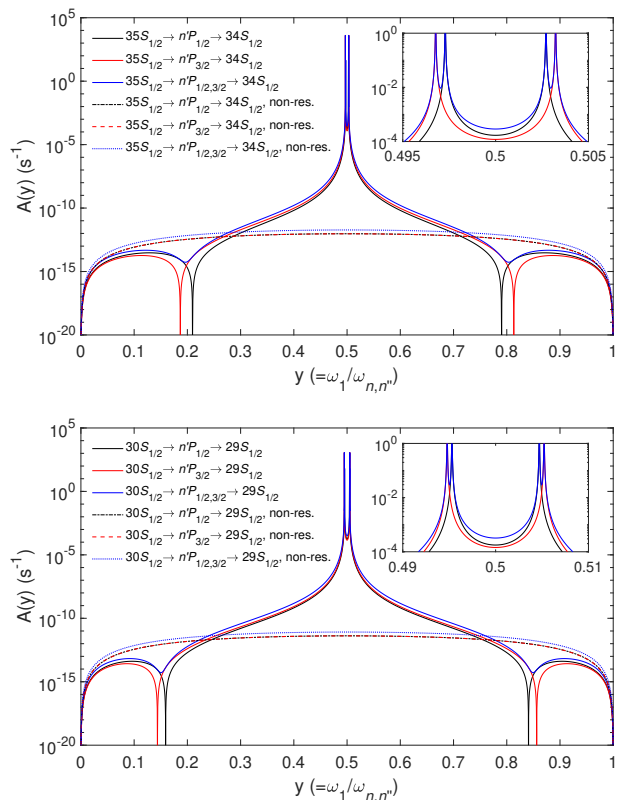


FIG. 5. Two-photon emission spectra for the $35S_{1/2} \rightarrow 34S_{1/2}$ (upper panel) and $30S_{1/2} \rightarrow 29S_{1/2}$ (lower panel) transitions. The corresponding frequencies $\omega_{n,n'}/2\pi$ are 181 and 295 GHz, respectively. The variable y is the single-photon frequency ω_1 with respect to the two-photon transition frequency $\omega_{n,n'} (= \omega_1 + \omega_2)$. The black and red lines represent the transitions via $n'P_{1/2}$ and $n'P_{3/2}$, respectively, whereas the blue line is the sum of these two. The dotted-dashed, dashed, and dotted lines represent the non-resonant spectra.

transitions through the $n'P_{1/2}$ and $n'P_{3/2}$ states, respectively. The sum of the two transitions, as the probability of two-photon decay, is shown in blue. The sharp and nearly Lorentzian peaks correspond to $n'P_j$ resonances, shifted, due to the spin-orbit interaction, as is clearly visible in the insets of Fig. 5. Furthermore, one sees the black and red curves suddenly drop to zero at certain frequencies. This behavior is caused by a destructive interference, resulting in the full cancellation of $M_{j'}^{(1)}$ and $M_{j'}^{(2)}$ terms, see Eq. (13), at specific values of y . In experiments, due to inhomogeneity and broadening, $A(y)$ will never be zero, but in our calculations, there is no other width than the natural linewidth.

Interestingly, the probability of emission of two identical photons is non-zero. The transition rate for $(n+1)S_{1/2} \rightarrow nS_{1/2}$ at $y = 0.5$ ($\omega_1 = \omega_2 = \omega_{n,n''}/2$) is equal to 1.70×10^{-4} , 1.20×10^{-4} , 1.77×10^{-4} , and $1.44 \times 10^{-4} \text{ s}^{-1}$, respectively, for the pair of quantum numbers (n, j') : $(34, \frac{1}{2})$, $(34, \frac{3}{2})$, $(29, \frac{1}{2})$, and $(29, \frac{3}{2})$.

We also investigated the non-resonant contribution to the two-photon spectral distribution $A(y)$, carrying out the summation in Eq. (13) over all states with energies $E_{n'} \geq E_n$ and $E_{n'} \leq E_{n''}$. One can identify, in Fig. 5, that it is small on the absolute scale compared with the peaks. However, the non-resonant terms noticeably increase the distant wings of the two-photon emission profiles (for about $y = 0$ and $y = 1$). After numerical integration, we obtained $A_t^{\text{non-res.}}(35S_{1/2} \rightarrow n'P_{1/2} \rightarrow 34S_{1/2} \text{ and } n' \neq 34) = 2.42 \times 10^{-13} \text{ s}^{-1}$, $A_t^{\text{non-res.}}(35S_{1/2} \rightarrow n'P_{3/2} \rightarrow 34S_{1/2} \text{ and } n' \neq 34) = 2.39 \times 10^{-13} \text{ s}^{-1}$, $A_t^{\text{non-res.}}(30S_{1/2} \rightarrow n'P_{1/2} \rightarrow 29S_{1/2} \text{ and } n' \neq 29) = 1.06 \times 10^{-12} \text{ s}^{-1}$, and $A_t^{\text{non-res.}}(30S_{1/2} \rightarrow n'P_{3/2} \rightarrow 29S_{1/2} \text{ and } n' \neq 29) = 1.05 \times 10^{-12} \text{ s}^{-1}$. Of course, within the non-relativistic treatment for the two-photon transition from $(n+1)S$ to nS of hydrogen-like atoms, only non-resonant contributions to the total two-photon decay rate matter because the energy levels of the same n but different l are degenerate. There are no real intermediate states; consequently, resonant contributions do not occur [53], in contrast to our case.

IV. CONCLUSIONS

We have accurately calculated the highly excited S , P , D , and F Rydberg states of the sodium atom within the Ritz variational method. The positive core-electron interaction was modeled by the parametric one-electron valence potential with spin-orbit coupling. We have determined the scalar and tensor polarizabilities for low and highly excited states and compared them with available experimental and theoretical results. After representing the polarizability as a series in powers of the effective principal quantum number, we found the leading expansion coefficients, allowing for rapid evaluation of α_0 and α_2 for arbitrary n and $l \leq 2$. As recently shown, utilizing the enormous polarizabilities of Rydberg states with the control of long-range interaction enables one to image the dynamics of ions embedded in a cold cloud of atoms [54]. We also calculated the largest Einstein coefficients for spontaneous and stimulated emission in the band of interest for photometric observations. From Fig. 3 and 4, one can immediately determine between which states the transitions take place for a given frequency. In general, the most probable Na transitions occur from the (n, l, j) state to the $(n, l-1, j-1)$ and $(n-1, l+1, j+1)$ states. We have also shown the emission of photons due to two-photon transitions from $30S_{1/2}$ to $29S_{1/2}$ and from $35S_{1/2}$ to $34S_{1/2}$.

The emphasis in our studies was on transitions in the microwave frequency range between 90 and 150 GHz. They may be helpful in calculating the expected LPRS signal flux density on Earth's surface at various microwave frequencies from the resulting laser-excited source in the sodium layer as a function of power and other properties of the two lasers and for precise relative radiometric and polarimetric calibration of ground-based microwave and millimeter-wave telescopes.

ACKNOWLEDGEMENTS

This work was partially supported at ITAMP by an NSF grant to Harvard University.

-
- [1] A. Osterwalder and F. Merkt, Using high Rydberg states as electric field sensors, *Phys. Rev. Lett.* **82**, 1831 (1999).
- [2] J. A. Sedlacek, A. Schwettmann, H. Kübler, R. Löw, T. Pfau, and J. P. Shaffer, Microwave electrometry with Rydberg atoms in a vapour cell using bright atomic resonances, *Nat. Phys.* **8**, 819 (2012).
- [3] H. Saßmannshausen, F. Merkt, and J. Deiglmayr, High-resolution spectroscopy of Rydberg states in an ultracold cesium gas, *Phys. Rev. A* **87**, 032519 (2013).
- [4] H. Q. Fan, S. Kumar, R. Daschner, H. Kübler, and J. P. Shaffer, Subwavelength microwave electric-field imaging using Rydberg atoms inside atomic vapor cells, *Opt. Lett.* **39**, 3030 (2014).
- [5] C. L. Holloway, J. A. Gordon, A. Schwarzkopf, D. A. Anderson, S. A. Miller, N. Thaicharoen, and G. Raithel, Sub-wavelength imaging and field mapping via electromagnetically induced transparency and Autler-Townes splitting in Rydberg atoms, *Appl. Phys. Lett.* **104**, 244102 (2014).
- [6] J. A. Gordon, C. L. Holloway, A. Schwarzkopf, D. A. Anderson, S. A. Miller, N. Thaicharoen, and G. Raithel, Millimeter wave detection via Autler-Townes splitting in rubidium Rydberg atoms, *Appl. Phys. Lett.* **105**, 024104 (2014).

- [7] H. Fan, S. Kumar, J. Sedlacek, H. Kübler, S. Karimkashi, and J. P. Shaffer, Atom based RF electric field sensing, *J. Phys. B: At. Mol. Opt. Phys.* **48**, 202001 (2015).
- [8] H. Fan, S. Kumar, J. Sheng, J. P. Shaffer, C. L. Holloway, and J. A. Gordon, Effect of vapor-cell geometry on Rydberg-atom-based measurements of radio-frequency electric fields, *Phys. Rev. Appl.* **4**, 044015 (2015).
- [9] M. T. Simons, J. A. Gordon, C. L. Holloway, D. A. Anderson, S. A. Miller, and G. Raithel, Using frequency detuning to improve the sensitivity of electric field measurements via electromagnetically induced transparency and Autler–Townes splitting in Rydberg atoms, *Appl. Phys. Lett.* **108**, 174101 (2016).
- [10] C. L. Degen, F. Reinhard, and P. Cappellaro, Quantum sensing, *Rev. Mod. Phys.* **89**, 035002 (2017).
- [11] C. L. Holloway, M. T. Simons, J. A. Gordon, P. F. Wilson, C. M. Cooke, D. A. Anderson, and G. Raithel, Atom-based RF electric field metrology: From self-calibrated measurements to subwavelength and near-field imaging, *IEEE Trans. Electromagn. Compat.* **59**, 717 (2017).
- [12] R. E. Sapiro, G. Raithel, and D. A. Anderson, Time dependence of Rydberg EIT in pulsed optical and RF fields, *J. Phys. B: At. Mol. Opt. Phys.* **53**, 094003 (2020).
- [13] L. Ma, M. A. Viray, D. A. Anderson, and G. Raithel, Measurement of dc and ac electric fields inside an atomic vapor cell with wall-integrated electrodes, *Phys. Rev. Appl.* **18**, 024001 (2022).
- [14] J. Yuan, W. Yang, M. Jing, H. Zhang, Y. Jiao, W. Li, L. Zhang, L. Xiao, and S. Jia, Quantum sensing of microwave electric fields based on Rydberg atoms, *Rep. Prog. Phys.* **86**, 106001 (2023).
- [15] C. W. Stubbs and J. L. Tonry, Toward 1% photometry: End-to-end calibration of astronomical telescopes and detectors, *Astrophys. J.* **646**, 1436 (2006).
- [16] J. E. Albert, D. Budker, K. Chance, I. E. Gordon, F. P. Bustos, M. Pospelov, S. M. Rochester, and H. R. Sadeghpour, A precise photometric ratio via laser excitation of the sodium layer - I. One-photon excitation using 342.78 nm light, *Mon. Notices Royal Astron. Soc.* **508**, 4399 (2021).
- [17] J. E. Albert, D. Budker, K. Chance, I. E. Gordon, F. P. Bustos, M. Pospelov, S. M. Rochester, and H. R. Sadeghpour, A precise photometric ratio via laser excitation of the sodium layer - II. Two-photon excitation using lasers detuned from 589.16 and 819.71 nm resonances, *Mon. Notices Royal Astron. Soc.* **508**, 4412 (2021).
- [18] J. E. Albert, D. Budker, and H. R. Sadeghpour, From atomic physics, to upper-atmospheric chemistry, to cosmology: A “laser photometric ratio star” to calibrate telescopes at major observatories, *Nat. Sci.* **2**, e20220003 (2022).
- [19] J. E. Albert, D. Budker, and H. R. Sadeghpour, (private communication) (2022).
- [20] The CMB Stage 4 (CMB-S4) project, supported by NSF, DOE, and other funding agencies, has main website <https://cmb-s4.org>, and its predicted primary scientific output is described in K. Abazajian *et al.*, CMB-S4: Forecasting constraints on primordial gravitational waves, *Astrophys. J.* **926**, 54 (2022).
- [21] D. E. Kelleher and L. I. Podobedova, Atomic transition probabilities of sodium and magnesium. A critical compilation, *J. Phys. Chem. Ref. Data* **37**, 267 (2008).
- [22] A. Kramida, Yu. Ralchenko, J. Reader, and NIST ASD Team, NIST Atomic Spectra Database (ver. 5.11), [Online]. Available at <https://physics.nist.gov/asd>. National Institute of Standards and Technology, Gaithersburg, MD. (2023).
- [23] T. F. Gallagher, L. M. Humphrey, R. M. Hill, W. E. Cooke, and S. A. Edelstein, Fine-structure intervals and polarizabilities of highly excited p and d states of sodium, *Phys. Rev. A* **15**, 1937 (1977).
- [24] C. Fabre, S. Haroche, and P. Goy, Millimeter spectroscopy in sodium Rydberg states: Quantum-defect, fine-structure, and polarizability measurements, *Phys. Rev. A* **18**, 229 (1978).
- [25] M. Pawlak, N. Moiseyev, and H. R. Sadeghpour, Highly excited Rydberg states of a rubidium atom: Theory versus experiments, *Phys. Rev. A* **89**, 042506 (2014).
- [26] M. Pawlak and H. R. Sadeghpour, Rydberg spectrum of a single trapped Ca^+ ion: A Floquet analysis, *Phys. Rev. A* **101**, 052510 (2020).
- [27] T. Dang, E. Klinger, F. P. Bustos, A. Wick-enbrock, R. Holzlöhner, and D. Budker, Satellite-assisted laser magnetometry with mesospheric sodium, *Opt. Continuum* **1**, 1263 (2022).
- [28] M. Marinescu, H. R. Sadeghpour, and A. Dalgarno, Dispersion coefficients for alkali-metal dimers, *Phys. Rev. A* **49**, 982 (1994).
- [29] M. Aymar, C. H. Greene, and E. Luc-Koenig, Multichannel Rydberg spectroscopy of complex atoms, *Rev. Mod. Phys.* **68**, 1015 (1996).
- [30] W. A. van Wijngaarden and J. Li, Polarizabilities of cesium S, P, D, and F states, *J. Quant. Spectrosc. Radiat. Transf.* **52**, 555 (1994).
- [31] A. Khadjavi, A. Lurio, and W. Happer, Stark effect in the excited states of Rb, Cs, Cd, and Hg, *Phys. Rev.* **167**, 128 (1968).
- [32] Z. Lai, S. Zhang, Q. Gou, and Y. Li, Polarizabilities of Rydberg states of Rb atoms with n up to 140, *Phys. Rev. A* **98**, 052503 (2018).
- [33] K. Miculis and W. Meyer, Phototransition of $\text{Na}(3p_{3/2})$ into high Rydberg states and the ionization continuum, *J. Phys. B: At. Mol. Opt. Phys.* **38**, 2097 (2005).
- [34] I. I. Sobelman, *Atomic spectra and radiative transitions*, 2nd ed., Atoms and Plasmas (Springer, 1996).
- [35] G. K. Woodgate, *Elementary atomic structure*, 2nd ed. (Clarendon Press, Oxford, 1983).
- [36] J. N. Dodd, The Einstein A and B coefficients, in *Atoms and light: Interactions*, Physics of Atoms and Molecules (Springer, 1991) pp. 89–95, 1st ed.
- [37] G. Breit and E. Teller, Metastability of hydrogen and helium levels, *Astrophys. J.* **91**, 215 (1940).
- [38] V. P. Demidov, Two-photon transitions between hyperfine-structure levels of the 1S state of the hydrogen atom, *Soviet Astron.* **5**, 816 (1962).
- [39] A. Dalgarno and D. R. Bates, Two-photon decay of singlet metastable helium, *Mon. Not. R. Astron. Soc.* **131**, 311 (1966).
- [40] G. Maroulis, Bonding and (hyper)polarizability in the sodium dimer, *J. Chem. Phys.* **121**, 10519 (2004).
- [41] J.-Y. Zhang and J. Mitroy, Long-range dispersion interactions. I. Formalism for two heteronuclear atoms, *Phys. Rev. A* **76**, 022705 (2007).
- [42] A. A. Kamenski and V. D. Ovsiannikov, Electric-field-induced redistribution of radiation transition probabilities in atomic multiplet lines, *J. Phys. B: At. Mol. Opt. Phys.* **39**, 2247 (2006).

- [43] C. R. Ekstrom, J. Schmiedmayer, M. S. Chapman, T. D. Hammond, and D. E. Pritchard, Measurement of the electric polarizability of sodium with an atom interferometer, *Phys. Rev. A* **51**, 3883 (1995).
- [44] C. Zhu, A. Dalgarno, S. G. Porsev, and A. Derevianko, Dipole polarizabilities of excited alkali-metal atoms and long-range interactions of ground- and excited-state alkali-metal atoms with helium atoms, *Phys. Rev. A* **70**, 032722 (2004).
- [45] R. W. Molof, H. L. Schwartz, T. M. Miller, and B. Bederson, Measurements of electric dipole polarizabilities of the alkali-metal atoms and the metastable noble-gas atoms, *Phys. Rev. A* **10**, 1131 (1974).
- [46] P. Hannaford, W. R. MacGillivray, and M. C. Standage, Coherent optical transient measurements of absolute and differential Stark shifts in atomic sodium, *J. Phys. B: At. Mol. Opt. Phys.* **12**, 4033 (1979).
- [47] K. C. Harvey, R. T. Hawkins, G. Meisel, and A. L. Schawlow, Measurement of the Stark effect in sodium by two-photon spectroscopy, *Phys. Rev. Lett.* **34**, 1073 (1975).
- [48] C. Fabre and S. Haroche, Observation of giant polarizabilities in atomic sodium Rydberg states, *Opt. Commun.* **15**, 254 (1975).
- [49] A. A. Kamenski and V. D. Ovsiannikov, Formal approach to deriving analytically asymptotic formulas for static polarizabilities of atoms and ions in Rydberg states, *J. Phys. B: At. Mol. Opt. Phys.* **47**, 095002 (2014).
- [50] C. Laughlin, On the accuracy of the Coulomb approximation and a model-potential method for atomic transition probabilities in alkali-like systems, *Phys. Scr.* **45**, 238 (1992).
- [51] W. P. Spencer, A. G. Vaidyanathan, D. Kleppner, and T. W. Ducas, Measurements of lifetimes of sodium Rydberg states in a cooled environment, *Phys. Rev. A* **24**, 2513 (1981).
- [52] S. Dyubko, M. Efimenko, V. Efremov, and S. Podnos, Microwave spectroscopy of *S*, *P*, and *D* states of sodium Rydberg atoms, *Phys. Rev. A* **52**, 514 (1995).
- [53] J. Chluba and R. A. Sunyaev, Two-photon transitions in hydrogen and cosmological recombination, *Astron. Astrophys.* **480**, 629 (2008).
- [54] C. Gross, T. Vogt, and W. Li, Ion imaging via long-range interaction with Rydberg atoms, *Phys. Rev. Lett.* **124**, 053401 (2020).